Journal of Hydroscience and Hydraulic Engineering
Vol. 27, No.1 May, 2009, 37-48

3D NUMERICAL PREDICTION FOR INTERACTION BETWEEN FREE-SURFACE FLOWS AND ELASTIC BODIES WITH MICS AND FINITE ELEMENT METHOD

By

Satoru Ushijima

Department of Civil and Earth Resources Engineering, Kyoto University, Kyoto-shi, 615-8540, Japan

and

Nozomu Kuroda

Department of Civil and Earth Resources Engineering, Kyoto University, Kyoto-shi, 615-8540, Japan

SYNOPSIS

A computational method has been proposed to predict the interactions between free-surface flows and elastic bodies included in the flows. A solid model, whose deformations due to fluid forces are solved with a finite element method, is introduced into the MICS, a computational method for incompressible multiphase fields. A solid object included in the flow is represented by multiple tetrahedron elements, through which fluid-solid interactions are taken into account on the basis of a tetrahedron sub-cell method. The developed computational method was applied to the experiments, in which four elastic plates were deformed due to the sloshing motions of free-surface flows in an accelerated tank. As a result, it was shown that the deformations of the plates and their interactions with the free-surface profiles are reasonably predicted with the present method.

INTRODUCTION

One of the most important engineering subjects is understanding the interactions between free-surface flows and flexible objects, such as the dynamic responses of the floating elastic structures and the variation of the fluid resistance forces of the flexible plants against free-surface flows. While many numerical investigations have been conducted for one and two-degree of freedom problems such as the oscillations of a cylinder in uniform flows (1), there are relatively few the numerical studies for multi-degree of freedom related to three-dimensional free-surface flows.

In the present study, a flexible object is represented by a T-type FEM model, in which the object is represented by multiple tetrahedron elements and its deformation is calculated with a finite element method (FEM). This T-type model is introduced into a computational method for a multiphase field, MICS (Multiphase Incompressible-flow solver with Collocated grid System). In the MICS, the free-surface flow including solid objects, consisting of gas, liquid and solid phases, is regarded as a multiphase field and it is modeled as a mixture of the immiscible and incompressible different fluids. The fluid-solid interactions are dealt with through the element of the T-type model and the fluid-cell in the MICS. Since no averaging procedures like turbulence models are introduced in the basic equations of MICS, it is applicable to turbulent flows around solid objects.

The prediction method was applied to the experimental results obtained in the sloshing motions in a water tank equipped with elastic plates. The oscillations of the water levels and the displacements of the elastic plates

are compared between experiments and predictions. By making comparisons, the validity of the prediction method is examined.

NUMERICAL PROCEDURES

Basic equations

It is important to deal with fluid-solid interactions accurately to predict the displacements of elastic bodies due to fluid forces in free-surface flows. The present numerical method deals with the free-surface flow including solid objects as a multiphase field consisting of the immiscible and incompressible different fluids. Thus, the governing equations are derived on the basis of the one-fluid model as shown by Ushijima et al. (2), which are the mass conservation equation in Eulerian description, the incompressible condition and the momentum equation in conservation form given as follows:

$$\frac{\partial \rho}{\partial t} + \frac{\partial}{\partial x_j}(\rho u_j) = 0 \tag{1}$$

$$\frac{\partial u_j}{\partial x_j} = 0 \tag{2}$$

$$\frac{\partial u_i}{\partial t} + \frac{\partial}{\partial x_j}(u_i u_j) = f_i - \frac{1}{\rho}\frac{\partial p}{\partial x_i} + \frac{1}{\rho}\frac{\partial}{\partial x_j}\left[\frac{\partial}{\partial x_j}(\mu u_i) + \frac{\partial}{\partial x_i}(\mu u_j)\right] \tag{3}$$

where t denotes time, x_i is the component of three-dimensional orthogonal coordinates and f_i is the acceleration component of the external forces. While the velocity component u_i is the mass-averaged value in the mixture of fluids, the density ρ, pressure p and viscous coefficient μ are defined as the volume-averaged values (2).

The basic equations are discretized in a collocated grid system and solved with a finite volume method. Firstly, the volume fraction of the object included in a fluid-cell is evaluated with the tetrahedron sub-cell method (3) and the volume-average physical properties are evaluated. Then, on the basis of the computational method for incompressible fluids (3), tentative velocity components are calculated at cell-center points with the C-ISMAC method (4). The derived velocity components are spatially interpolated on the cell-boundaries and pressure computations are performed with the C-HSMAC method (5). The free-surface profiles are calculated from Eq.1 with a non-diffusion filter.

T-Type FEM Model

In the present study, the solid object included in a free-surface flow is assumed to be an elastic body. It is important to calculate accurately the deformation as well as the acceleration and the velocity at each point of the body in order to predict the interactions between fluids and flexible objects. For this purpose, a T-type FEM model is introduced into the MICS. In the T-type model, as shown in Fig.1, an elastic object is represented by multiple tetrahedron elements. Each element has 10 nodes, which is called a quadratic iso-parametric element. Since the elements are independent of the fluid cells, its number can be determined in accordance with the shape of the object.

The fluid forces acting on the nodes are used to calculate their displacements. When the displacements depend on time, two sets of additional forces should be taken into account in addition to the elastic forces due to deformations; an inertia force and a damping force. While the inertia force is given by the product of mass and the acceleration vector, the damping force is caused by the internal frictional resistances against the motions,

which is assumed to be linear with the velocity of the body. Thus, the basic equation of the dynamic behavior of an elastic object is given by

$$M\ddot{\boldsymbol{d}} + C\dot{\boldsymbol{d}} + K\boldsymbol{d} = \boldsymbol{f}_e \tag{4}$$

where $\boldsymbol{d}$ denotes a displacement vector, M is a lumped mass matrix, C is a lumped damping matrix, K is an assembled stiffness matrix and $\boldsymbol{f}_e$ is the external force vector.

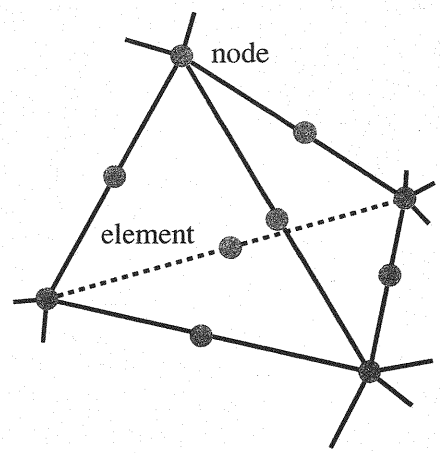

Fig. 1 Tetrahedron element and nodes

The assembled stiffness matrix K is constructed from the element stiffness matrices K_e. The K_e is calculated by the following relationship:

$$K_e = \int_V B^T D B dV \tag{5}$$

where V is a tetrahedron element and B^T is the transposed matrix of B, which is a 6×30 matrix defined in the following equation:

$$\boldsymbol{\epsilon} = B\boldsymbol{d} \tag{6}$$

where $\boldsymbol{\epsilon}$ is a strain vector. The matrix D in Eq.5 is a 6×6 matrix, whose elements are determined with the Young's modulus, modulus of rigidity and Poisson ratio, defined in the following form:

$$\boldsymbol{\sigma} = D\,\boldsymbol{\epsilon} \tag{7}$$

where $\boldsymbol{\sigma}$ is a stress vector. Eq.5 is calculated by numerical integration over the standard tetrahedron element with 4 integral points (6).

Applying the Euler explicit method to Eq.4, the velocity vector $\dot{\boldsymbol{d}}^{n+1}$ is calculated from the following equation:

$$\dot{\boldsymbol{d}}^{n+1} = \dot{\boldsymbol{d}}^{n} + M^{-1}(\boldsymbol{f}_e^n - C\dot{\boldsymbol{d}}^{n} - K\boldsymbol{d}^n)\Delta t \tag{8}$$

Since the matrices M^{-1} and C have diagonal forms, the products of the matrix and vector are easily calculated. The stiffness matrix K, on the other hand, must be constructed from the element stiffness matrices K_e. In order

to simplify the numerical procedures, element-by-element method (7) is employed. Thus, the product $K\boldsymbol{d}$ is calculated directly without composing K using the following procedures:

```
v(:, :) = 0.0d0
do ne = 1, nttr ! (A)
   do nt1 = 1, 10 ! (B)
      get the node number nd1 for nt1
      do nt2 = 1, 10 ! (C)
         get the node number nd2 for nt2
         do j = 1, 3 ! (D)
            do i = 1, 3 ! (E)
               v(i, nd1) = v(i, nd1) &
                 + ke(i, j, nt1, nt2, ne) &
                 * d(j, nd2) ! (F)
            enddo
         enddo
      enddo
   enddo
enddo
```

The variables nt1 and nt2 stand for local 10 node numbers included in an element, while nd1 and nd2 are global node numbers for all nodes in the computational region.

The iteration (A) is preformed for all elements, (B) and (C) for the node of a tetrahedral element, (D) and (E) for three dimensional components. In the numerical process (F), the product of the element stiffness matrix K_e and the element displacement vector $\boldsymbol{d}$ is added to v. After the above numerical procedures, the one-dimensional array v contains the elements of the product $K\boldsymbol{d}$.

Applying the Euler implicit method to Eq.8, the displacements at nodes $\boldsymbol{d}^{n+1}$ are calculated with the following relationship:

$$\boldsymbol{d}^{n+1} = \boldsymbol{d}^{n} + \dot{\boldsymbol{d}}^{n+1}\Delta t \tag{9}$$

Interaction between Fluid and Object

The fluid forces acting on the object are determined from the pressure and viscous terms of Eq.3. It is noted in the present method that the interactions between fluids and objects are evaluated from the volume integral rather than the surface integral. In the T-type solid model, the fluid forces are calculated at the nodes. Thus, the fluid force is firstly estimated in a portion of the tetrahedron element included in a fluid-cell, as shown in Fig.2, and then it is distributed to the nodes. In Fig.2, the tetrahedron elements and a three-dimensional fluid-cell are schematically shown as triangles with only four nodes and a rectangle respectively.

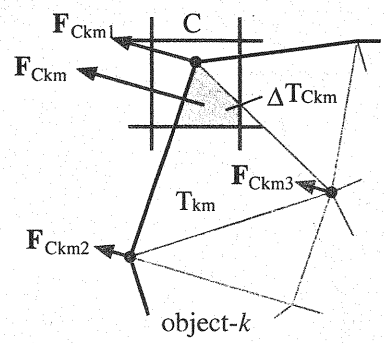

Fig. 2 Estimation of fluid force acting on object

In Fig.2, $\boldsymbol{F}_{Ckm}$ indicates the fluid force vector acting on a portion of the element T_{km} of the object$-k$ included in a fluid-cell C. The x_i component of $\boldsymbol{F}_{Ckm}$, which is indicated as $\boldsymbol{F}_{Ckmi}$, is calculated with a portion of the element volume ΔT_{Ckm} included in the fluid-cell C and the density ρ_{bk} of the object$-k$ as

$$F_{Ckmi} = \rho_{bk}\Delta T_{Ckm}\left[-\frac{1}{\rho}\frac{\partial p}{\partial x_i} + \frac{1}{\rho}\frac{\partial}{\partial x_j}\left\{\frac{\partial}{\partial x_j}(\mu u_i) + \frac{\partial}{\partial x_i}(\mu u_j)\right\}\right] \tag{10}$$

where ΔT_{Ckm} is estimated with the tetrahedron sub-cell method (8).

The fluid force vector $\boldsymbol{F}_{Ckm}$ calculated from Eq.10 is distributed to the nodes. As shown in Fig.2, $\boldsymbol{F}_{Ckm}$ is transformed to $\boldsymbol{F}_{Ckmj}$ at 10 nodes of the tetrahedron element ($j = 1, \cdots, 10$) by applying weighting function related to the distances from the nodes to the center of the fluid-cell. For each node, the external force vector $\boldsymbol{f}_e$, included in Eq.4, is determined from the summation of $\boldsymbol{F}_{Ckmj}$ taken over related elements and fluid-cells.

On the other hand, the response of the dynamic behaviors of the object is taken into account in the multiphase field, as shown in Fig.3. Although the elements and fluid-cell are schematically shown in Fig.3, their actual geometry is three dimensional and each element has 10 nodes. The velocity vector $\boldsymbol{v}_{km}$ of the tetrahedron element is determined as the average value of those defined at 10 nodes, which are equivalent to the node velocity vector $\boldsymbol{v}_{kmj}$ in Fig.3 ($j = 1, \cdots, 10$). The contribution of the element of T_{km} to the fluid-cell C is then determined with $\boldsymbol{v}_{km}$, density and volume fraction ΔT_{Ckm}. Thus the velocity at the center of the fluid-cell in the multiphase field is determined as the following mass-averaged value:

$$\boldsymbol{u} = \frac{1}{m_C}\left(m_f \boldsymbol{u}_f + \sum_k \sum_m \rho_{bk}\Delta T_{Ckm}\boldsymbol{v}_{km}\right) \tag{11}$$

where m_C and m_f are total mass in the fluid-cell and the mass of gas and liquid phases, respectively. The velocity vector of the mixture of gas and liquid phases is given by $\boldsymbol{u}_f$.

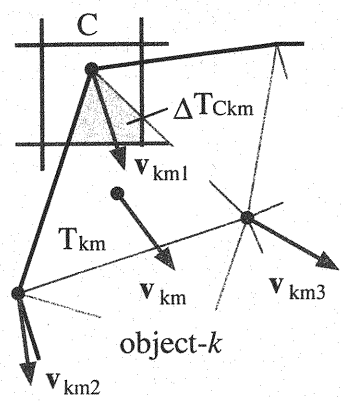

Fig. 3 Transformation from object motion to velocity in multiphase field

HYDRAULIC EXPERIMENTS AND APPLICABILITY OF PREDICTION METHOD

Sloshing Experiments with Elastic Plate

In order to confirm the applicability of the prediction method, hydraulic experiments were carried out with an accelerated tank, in which four elastic plates are deformed due to the sloshing motion of water. The length L and width b of the water tank shown in Fig.4 are 190 mm and 60 mm respectively. Four elastic plates are fixed on the bottom of the tank. The plates are made of a kind of sponge with the specific density of 0.255. The lengths h_b, b_1 and b_2 are 100 mm , 15 mm and 30 mm respectively and its thickness is 10 mm. The distances d_1 and d_2 are 45 mm and 35 mm respectively. It was confirmed that the plates can be treated as perfect elastic bodies through the relationship between the imposed loads and the displacements.

When the horizontal acceleration is given to the tank, large oscillations of the water surface and fluid flows occur, which cause deformation of the plates. In the experiments, the initial water depth was set at h_0 and the positive acceleration a_x was added in x direction for a period of time Δt_a. Following this motion, the negative acceleration $-a_x$ was given for Δt_a and the tank was stopped. The free-surface motions and deformation of the plates were recorded by a video camera. The acceleration a_x was 1.0 m/s^2 and Δt_a was 0.2 sec. Three conditions were set up for the initial water depths h_0 in the present experiments; 75 mm (case-H75), 100 mm (case-H100) and 125 mm (case-H125).

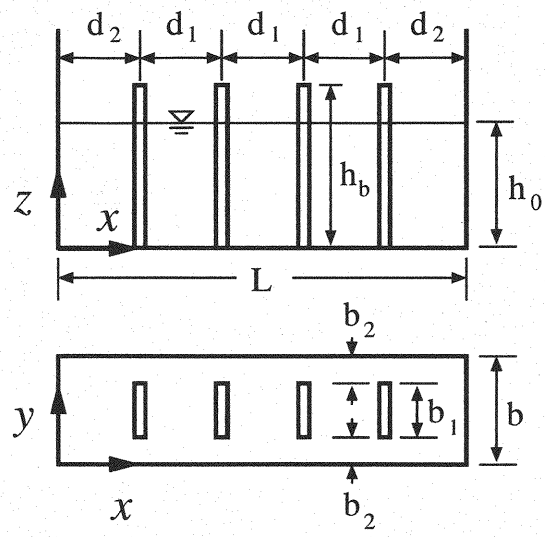

Fig. 4 Water tank used in experiments (side and plane views)

Conditions of computations

In the computations, a fluid-cell was the 5 × 5 × 5 mm cube and they were set for all regions inside of the tank, including water, air and elastic plate regions. The kinematic viscosities of water and air were set at 1.0×10^{-6} and 1.0×10^{-5} m^2/s respectively. Their densities were 1.0×10^3 and 1.0 kg/m^3 respectively. The elastic plate was represented by 184 tetrahedron elements with 441 nodes using the T-type FEM model. The Young's modulus of the plates was 3.5×10^5 Pa and the damping coefficient per unit volume was set at 2.0×10^4 N s/m/m^3. On the boundary surfaces of the computational volume, non-slip conditions are applied to velocity and normal gradients of the pressure are set at zero.

Comparison between Experiments and Calculations

Fig.5 shows the predicted free-surface profiles and plate deformations for case-H75. In this case, the top of the plates are always located above the water surfaces. Similarly, Fig.6 and Fig.7 show the calculated results for case-H100 and case-H125 respectively. In these figures, the iso-lines for the absolute values of vorticities arising near the plates are also indicated. The red and blue colors show the high and low vorticities, respectively. It can be seen that the vorticities become larger near the top of the plates. The free-surface oscillation and the accompanied deformation of the plates are predicted reasonably well in these results.

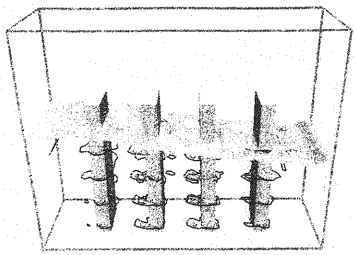

(a) $t = 0.2$ (s)

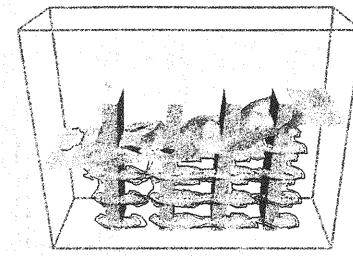

(b) $t = 0.4$ (s)

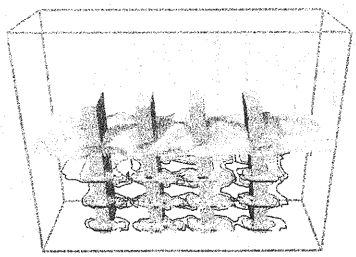

(c) $t = 0.6$ (s)

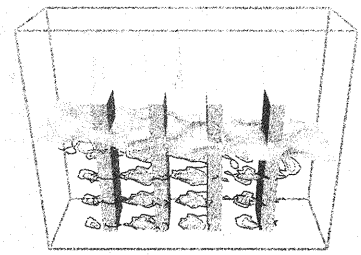

(d) $t = 0.8$ (s)

Fig. 5 Predicted results (case-H75)

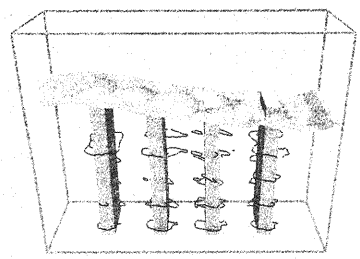

(a) $t = 0.2$ (s)

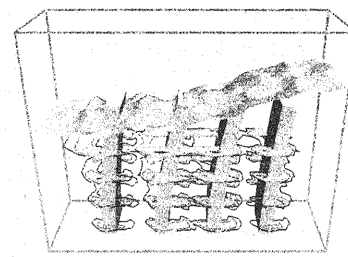

(b) $t = 0.4$ (s)

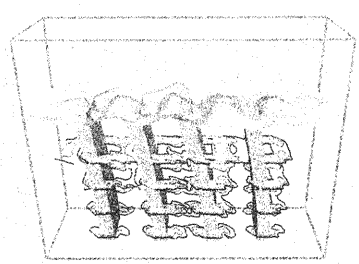

(c) $t = 0.6$ (s)

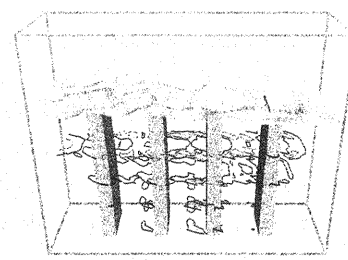

(d) $t = 0.8$ (s)

Fig. 6 Predicted results (case-H100)

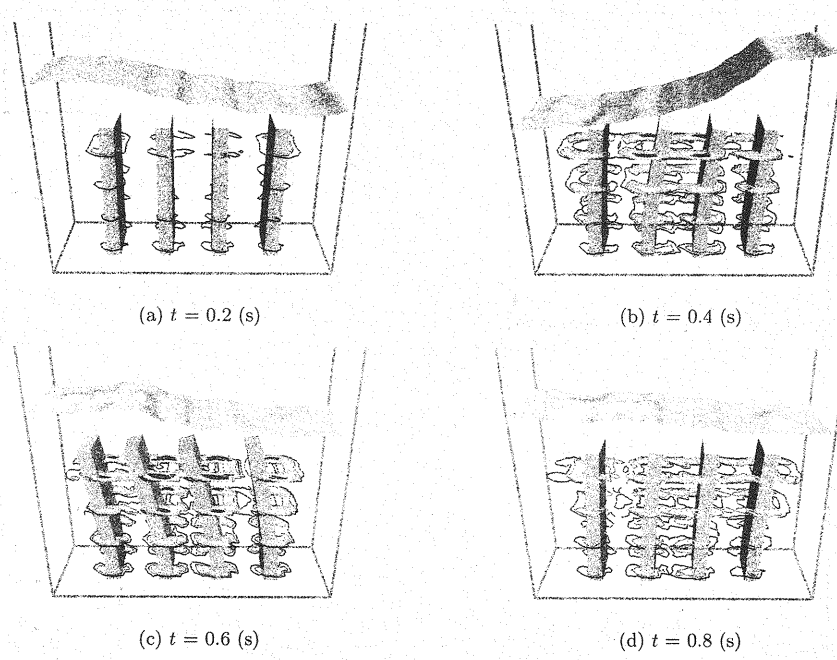

(a) $t = 0.2$ (s)　　(b) $t = 0.4$ (s)

(c) $t = 0.6$ (s)　　(d) $t = 0.8$ (s)

Fig. 7 Predicted results (case-H125)

Fig.8 shows the time histories of the water levels η_0 and η_L on the both ends of the tank, $x = 0$ and L, as well as the displacements d_t of the top of one plate located in the inner side of four plates. The predicted water levels generally agree with the measured maximum waver levels η_m. The phase of the predicted displacement d_t shift by about $\pi/4$ compared with those of the water levels η_0 and η_L. This tendency means that the maximum deformations of the plates are mainly caused when the flow velocities reach the maximum values.

Fig.9 shows the time histories of d_t obtained in the predictions and experiments. The displacements of the inner plates, indicated as " (in) " in Fig.9, are larger than those of the outer ones, indicated as " (out) " in the same figure. Since the flow velocities near the edges of the tank are relatively small, the displacements of the outer plates decrease compared with the inner ones. Including this tendency, the predicted results generally agree with the experimental ones.

Both in the experiments and calculations, sloshing motions near the first-mode were observed as shown in Fig.8 to Fig.9. The natural time period of the first-mode sloshing is about 0.51 second for case-H100, while the natural time period of the elastic plate itself is about 0.16 sec. Since the time period of the plate oscillation is close to that of the sloshing, it can be thought that the oscillations of the plates are mainly caused by the fluid motions rather than its natural frequency.

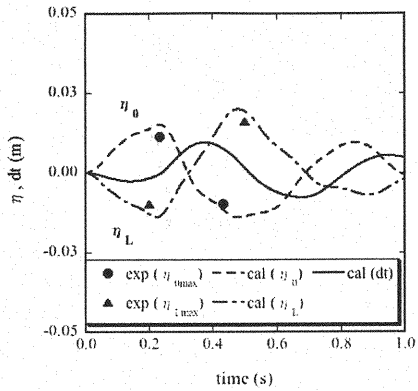

(a) case-H75

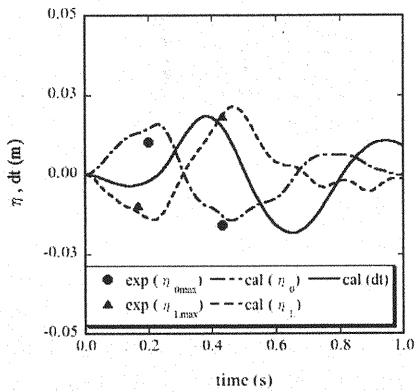

(b) case-H100

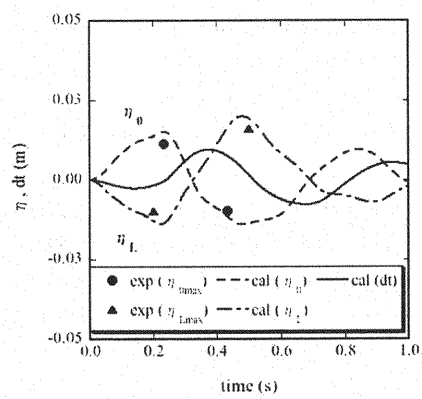

(c) case-H125

Fig. 8 Time histories of water levels and plate displacements

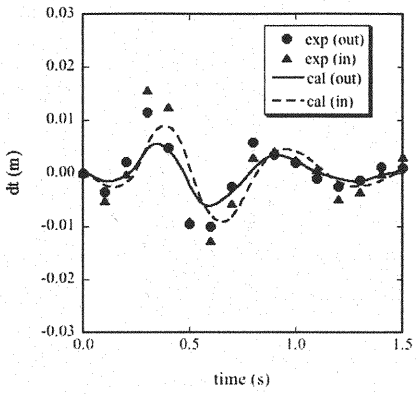

(a) case-H75

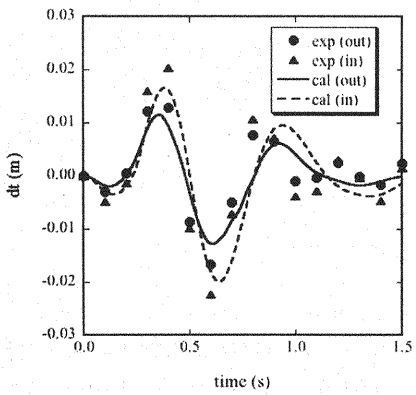

(b) case-H100

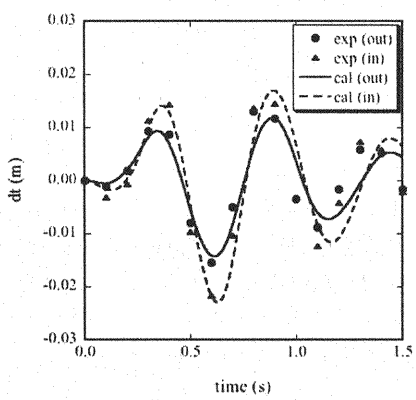

(c) case-H125

Fig. 9 Time histories of plate displacements

CONCLUSIONS

In this study, a computational method was developed to predict the interactions between free-surface flows and the deformations of elastic objects. A T-type FEM model, in which the deformations of elastic bodies are calculated with FEM, was introduced into the MICS, a computational method for a multiphase field. The interactions between fluids and solid objects are adequately taken into account through the tetrahedron sub-cell method. The developed computational method was applied to the experiments, in which four elastic plates were deformed due to the sloshing motions of free-surface flows in an accelerated tank. As a result, it was shown that the deformations of the plates and their interactions with the free-surface profiles can be predicted fairly well with the present method.

REFERENCES

1. Izumi, H., Taniguchi, N., Kawata, Y. and Kobayashi, T.: Three-dimensional flow analysis around a circular cylinder, *Trans. JSME, B*, Vol. 66, No. 644, pp. 1013–1020, 2000.

2. Ushijima, S., Yamada, S., Fujioka, S. and Nezu, I.: Prediction method (3D MICS) for transportation of solid bodies in 3D free-surface flows, *JSCE Journal*, Vol. 810/II-74, pp. 79–89, 2006.

3. Ushijima, S., Takemura, M., Yamada, S. and Nezu, I.: Computational method for multiphase incompressible flows (MICS) and its applicability to particle-laden liquid flows, *JSCE Journal*, No. 740/II-64, pp. 121–130, 2003.

4. Ushijima, S. and Nezu, I.: Higher-order implicit (C-ISMAC) method for incompressible flows with collocated grid system, *JSCE Journal*, No. 719/II-61, pp. 21–30, 2002.

5. Ushijima, S., Okuyama, Y., Takemura, M. and Nezu, I.: Parallel computational method for pressure field in incompressible flows on 3D curvilinear coordinates, *Annual Journal of Hydraulic Engineering, JSCE*, Vol. 47, pp. 385–390, 2003.

6. Hammer, P. C., Marlowe, O. P. and Stroud, A. H.: Numerical integration over symplexes and cones, *Math. Tables Aids Comp*, Vol. 10, pp. 130–137, 2007.

7. Barragy, E. and Carey, G. F.: A parallel element-by-element solution scheme, *Int. J. Num. Meth. Engrg.*, Vol. 26, pp. 2367–2382, 1988.

8. Ushijima, S.: Multiphase-model approach to predict arbitrarily-shaped objects moving in free surface flows, *Proc of APCOM'07 - EPMESC XI*, pp. MS41-3-1, 2007.

APPENDIX-NOTATION

The following symbols are used in this paper:

B = matrix of stress-displacement relations;

C = lumped damping matrix;

D = matrix of stress-strain relations;

$\boldsymbol{d}$ = displacement vector;

F^i_{Ckm} = fluid force acting on ΔT_{Ckm} in x_i direction;

$\boldsymbol{f}_e$ = external force vector;

f_i = acceleration component of external force;

K = assembled stiffness matrix;

K_e = element stiffness matrix;

M = lumped mass matrix;

m_c = total mass in the fluid-cells;

m_f = mass of gas and liquid phases;

p = volume-averaged pressure;

t = time;

u_i = mass-averaged velocity component in x_i direction;

$\boldsymbol{u}_f$ = velocity vector of gas and liquid phases;

$\boldsymbol{v}_{km}$ = velocity vector of tetrahedron element;

x_i = orthogonal coordinates;

Δt = time increment;

ΔT_{Ckm} = portion of the element volume included in the fluid-cell C ;

$\boldsymbol{\epsilon}$ = strain vector;

μ = volume-averaged coefficient of viscosity;

ρ = volume-averaged density;

ρ_{bk} = density of object$-k$; and

$\boldsymbol{\sigma}$ = stress vector.

(Received Jul 16, 2008 ; revised Nov 21, 2008)